FOURTEENTH EUROPEAN ROTORCRAFT FORUM

Paper No. 60

AUTOMATIC VIBRATION REDUCTION AT A FOUR BLADED HINGELESS MODEL ROTOR - A WIND TUNNEL DEMONSTRATION

G. LEHMANN
R. KUBE

DEUTSCHE FORSCHUNGS- UND VERSUCHSANSTALT
FÜR LUFT- UND RAUMFAHRT E.V.,
INSTITUT FÜR FLUGMECHANIK, BRAUNSCHWEIG, GERMANY

20-23 September, 1988
MILANO, ITALY

ASSOCIAZIONE INDUSTRIE AEROSPAZIALI
ASSOCIAZIONE ITALIANA DI AERONAUTICA ED ASTRONAUTICA

AUTOMATIC VIBRATION REDUCTION AT A FOUR BLADED HINGELESS MODEL ROTOR - A WIND TUNNEL DEMONSTRATION

G. Lehmann
R. Kube

Deutsche Forschungs- und Versuchsanstalt
für Luft- und Raumfahrt e.V.,
Institut für Flugmechanik, Braunschweig, Germany

Abstract

As a part of a program named ACTHOR, the synonym for Active Control Technology for Helicopter Operation and Research, a wind tunnel demonstration was performed to show the capabilities of a digital system for automatic vibration reduction by means of Higher Harmonic Control (HHC).

The implemented adaptive controller is based on a Kalman Filter which showed an excellent identification behaviour without any tendency of instabilities. This online identification led to a stable operation of the controller over the full speed range at trimmed and untrimmed flight conditions and made him in addition capable to handle different feedback signals without changing software. It was only necessary to switch from one sensor to another, whereupon the system only needed a short adaption time to work with optimal performance again.

While the first part of this paper deals with some theoretical aspects of the control algorithm and its realization on a digital computer system, in the second part the wind tunnel tests are described and the controller behaviour is demonstrated by aid of test results. As a further topic the T-matrix which characterizes the actual rotor state is evaluated and discussed for various flight conditions.

1. Introduction

The vibration level of a helicopter compared with this one of a fixed wing aircraft is very high and represents a considerable stress for material and crew. This effects the passenger's comfort as well as the flight security, so intensive work has been done in the past to improve the helicopter behaviour in this respect. Because the initial success of passiv damping elements (Ref. [1]) could not be carried on in the desired manner, it was not possible to meet the more and more stringent vibration requirements coupled with the wish of a higher and higher cruising speed. Therefore weight effective control systems had to be developped which perform a significant vibration reduction throughout the whole flight envelope.

Analytical studies have shown, that these goals can be achieved by means of HHC, because this method suppresses helicopter vibrations at the source by using a higher harmonic blade root pitch to modify the unsteady loads of the rotor blades. The generation of the related HHC actuator signals requires an electronical system which utilizes the measured vibration components as feedback variables and subjects them to a more or less complex control algorithm.

A few years ago, the real time enforcement of this task was only possible by means of analog circuits, working on the one hand very quickly but on the other hand being affected with the wellknown disadvantages like high costs, offset and drift. Only the evolution of the highspeed, lightweight microcomputers made a digital realization of HHC possible which allows a software implementation of the control algorithm and therefore a very easy adaption to the experimental system. Because this flexibility is a great advantage for wind tunnel testing, the DFVLR Institut for Flight Mechanics decided to design a digital control system too, allowing an open loop- as well as a closed loop operation. The tests conducted with this system in conjunction with the DFVLR rotor test stand at the German-Dutch wind tunnel (Fig. 1) showed a very stable behaviour and a short response time of the controller so that successfull flight tests appear to be within reach.

2. Control Algorithm and HHC Signal Generation

For closed-loop wind tunnel testing a control algorithm is required determining the optimal HHC-inputs for the actual flight condition. The result of this task depends on the structure of the controller as well as on its adjustement which, in the case of HHC, is very difficult due to the time-variing state of the rotor. Therefore an adaptive control algorithm appears to be necessary identifying the rotor state and adjusting himself in every cycle.

In the past this kind of controller has been investigated intensively in order to achieve a stable behaviour and a good performance even in transient maneuvers (Ref [2]). Although two controller types are imaginable, one working in the time domain and one working in the frequency domain, for an application in conjunction with HHC, only the latter one seems to be suited, because the main portion of the helicopter vibrations is the 4/rev component, thus a force of periodical nature. Therefore it is sufficient to minimize the real- and imaginary part of this component leading to a controller which works in the frequency domain and determines the amplitudes and phase shifts of the actuator signals.

In our case, a linear relationship between the vibration change and the HHC input change is assumed, leading to the so called "local model"

$$\underline{z}(kT_s) - \underline{z}((k-1)T_s) = \underline{T} \cdot (\underline{\Theta}(kT_s) - \underline{\Theta}((k-1)T_s))$$

where

$\underline{z}(kT_s)$	is a vector including the cosine and sine components of the 4/rev part of the vibrations in the fixed system,
$\underline{\Theta}(kT_s)$	is a vector including the cosine and sine components of the higher harmonic control signals in the rotating system,
k	is the sample index,
T_s	is the sample period
$\underline{T}$	is the rotor state matrix.

The T-matrix is estimated recursively by a Kalman filter and then is passed to a Minimum Variance Controller which minimizes the quadratic quality criterion

$$J = \underline{z}^T((k+1)T_s) \cdot \underline{W}_z \cdot \underline{z}((k+1)T_s) + \underline{\Theta}^T((k+1)T_s) \cdot \underline{W}_\Theta \cdot \underline{\Theta}((k+1)T_s).$$

This criterion incorporates the balancing matrices $\underline{W}_z$ and $\underline{W}_\Theta$ making it possible to influence the controller behaviour in a wide range.

If for example the elements of $\underline{W}_\Theta$ are set to a high value, the controller will act carefully, whereas a more aggressive behaviour can be expected if $\underline{W}_\Theta$ is set to zero.

On the other hand $\underline{W}_z$ allows an individual balancing of the different sensor signals which in the case of the aspired flight tests makes it possible to minimize the vibrations of specific helicopter components and to find out the sensor configuration mostly increasing the passenger's comfort.

Fig. 2 depicts schematically the control algorithm which can be carried out up to now in less than a half rotor revolution. The picture makes clear, that, in addition to the essential adaptive control algorithm, the vibration signals have to be transformed from the time- to the frequency domain, whereas the control parameters, in return, have to be transformed from the frequency to the time domain.

In order to allow a digital accomplishment of these tasks and to avoid analog components within the HHC-system, two algorithms have been developed which are well suited for a real-time enforcement because they require the performance of only a few mathematical operations.

In the case of the harmonic analysis this was achieved by determining only the Fourier coefficient associated with the 4/rev vibration component on the one hand and , on the other hand, by using a recursive calculation algorithm. This algorithm is based upon the wellknown formulas

$$a_4(kT) = 2/N \sum_{i=k-N+1}^{k} y(iT) \cdot \sin(4 \cdot 2\pi f_R \cdot iT) = 2/N \sum_{i=k-N+1}^{k} a(iT) = 2/N \cdot a_s \qquad (1)$$

$$b_4(kT) = 2/N \sum_{i=k-N+1}^{k} y(iT) \cdot \cos(4 \cdot 2\pi f_R \cdot iT) = 2/N \sum_{i=k-N+1}^{k} b(iT) = 2/N \cdot b_s \qquad (2)$$

with

f_R	as rotational frequency,
$N \cdot T$	as signal period,

from which it can be derived, that the coefficients of two consecutive sample points kT and (k+1)T only differ by the elements a((k-N+1)T) and a((k+1)T) respectively b((k-N+1)T) and b((k+1)T). Thus if the elements a(iT) and b(iT) of (1) and (2) are stored in two arrays, for example called ABUF and BBUF, it becomes possible to determine the coefficients $a_4((k+1)T)$ and $b_4((k+1)T)$ by simply subtracting the elements a((k-N+1)T) and b((k-N+1)T) from a_s and b_s, adding a((k+1)T and b((k+1)T) to the result before multiplying it with 2/N. Because a((k-N+1)T) and b((k-N+1)T) are not used anymore, they can be substituted by a((k+1)T) and b((k+1)T) guaranteeing a constant amount of required memory space and making it possible to select the actual element of ABUF and BBUF by the rotor azimuth ψ. In the case of the DFVLR rotor test stand, this can be realized with the implemented angle encoder which puts out an integer value proportional to ψ being used as pointer to ABUF and BBUF.

The algorithm can be speeded up further if the trigonometrical functions which are necessary for the calculation of the elements a(iT) and b(iT) of (1) and (2) are determined in advance for all sample points within one rotor revolution and are stored in two arrays called SBUF and CBUF. Thereby it becomes possible, that during operation of the system, the elements corresponding to the actual rotor azimuth ψ only have to be selected by means of the above already mentioned digital angle encoder, which avoids the time consuming online calculation of a trigonometrical function. This leads to an algorithm which comprises a smaller amount of mathematical operations than a computation of the formulas (1) and (2) for the sample point (k+1)T would entail.

Fig. 3 shows schematically the operation of the algorithm, whereas Fig. 4 makes clear, that an acceptable behaviour can be achieved even if only 32 sample points per rotor revolution are taken into account.

Nevertheless the response of this algorithm can be speeded up by correcting the actual estimates in the manner

$$ak_4((k+1)T) = a_4(kT) + fk \cdot (a_4((k+1)T) - a_4(kT))$$

and

$$bk_4((k+1)T) = b_4(kT) + fk \cdot (b_4((k+1)T) - b_4(kT))$$

where fk is eligible and therefore adaptable to the actual application. Fig. 5 shows the result of this modification and depicts, that this form of the algorithm achieves a faster response than this one mentioned before, especially if the 4/rev input signal changes smoothly which is typical for an application in conjunction with HHC.

As well as for the time to frequency conversion of the vibration signals, a time-efficient algorithm was developped for the HHC signal generation too being based upon the fact, that a 3-, 4- and 5/rev blade pitch angle can be attained by actuator signals with a constant frequency of $4f_R$, where f_R is the rotational frequency of the rotor. As can be seen from [3], the generated frequency in the rotating system depends only on the phase shifting of the actuator signals which, in the case of the DFVLR rotor test stand, have to be 0° for a 4/rev blade pitch angle and + 120° respectively − 120° for the generation of the 3rd and 5th harmonic. These values result from the arangement of the actuators being displaced by 120° against each other and lead in the first case to a parallel shifting of the swashplate's orthogonal vector whereas in the other cases the peak of this vector moves on a circle with respectively against the turning direction of the rotor.

In order to generate the corresponding 4/rev actuator signals with only a small software-overhead, the values of a cosine with amplitude one are calculated again in advance for all sample points within one rotor revolution and are stored in an array called CONTROL BUFFER (Fig. 6) which during operation of the system is adressed by three pointers depending on the rotor azimuth and the phase shifting of the actuator signals. In this way, three cosine signals with amplitude one are generated being passed to the first input of three external multipliers, whereas the second input is controlled by the amplitudes of the dynamic actuator signals.This leads to control signals which are necessary for the desired higher harmonic blade pitch angle.

3. Hardware Configuration

The HHC system which in detail is described in [4] consists mainly of two digital computers. They are entitled with Signal Processor (SP) and Adaptive Control Processor (ACP), and share the tasks required for an automatic vibration reduction as shown in Fig. 7. It can be seen, that the ACP accomplishes the adaptive control algorithm, whereas the SP performs the signal-I/O and the signal conditioning, i.e., the identification of the 4/rev vibration component by means of the

above mentioned algorithm. These values are passed to the ACP via a dual port memory which allows a parameter transfer with only a small software overhead thus avoiding to spend a lot of time for the performance of a non-essential task.

The ACP calculates the amplitudes and phase shifts of the 3-, 4- and 5/rev blade pitch angle required for the minimization of the 4/rev vibration component and passes them, again via the dual port memory, to the SP which computes the associated HHC signals and supperposes them to the conventional control values.

The response of the rotor in dependance of the HHC inputs can be observed by strain gauges which are implemented on the rotor as shown in Fig. 8 making it possible to determine the flapping, lagging and torsional motion of the blades.

In addition, the seven load cell systems which connect the upper and the lower plate of the rotor balance as depicted in Fig. 9 make it possible to measure the vibrations in the fixed system. These elements consist of a strain gauge part measuring the static forces and a pieco electrical part measuring the dynamic forces and can be used as feedback signals as well as the three additional accelerometers which are implemented close to the rotor (Fig. 9) giving a possibility to test the controller in conjunction with a sensor configuration which can also be used during flight tests.

Fig. 10 shows a photograph of the complete computer system including the peripheral devices which allow an observation and manipulation of the controller behaviour and an easy operation during the wind tunnel tests.

The SP, for example, is equiped with a potentiometer panel, giving the possibility to adjust the amplitudes and phaseshifts of the 3-, 4-and 5/rev blade pitch angle in the open loop mode of the system and displaying the above mentioned quality criterion J in an analog form.

Other important system parameters, like the real- and imaginary parts of the 4/rev vibration components for example, are putted out via the so called "I/O- Panel" which, in addition, allows to adjust the balancing matrices $\underline{W}_z$ and $\underline{W}_\Theta$ of the quality criterion by potentiometers thus making an online tuning of the controller possible.

Via the provided operating-panel connected with both processors, the SP and the ACP, the computer system can be initialized, started, stopped and switched from one mode to another, i.e. the open loop-, closed loop-, fixed gain- and adaptive mode.

Besides these panels an intelligent terminal, based upon a Personal Computer was implemented which is linked to the ACP and puts out important system parameters, like the T-matrix, the amplitudes and phase shifts of the HHC blade pitch angles, the rotor components etc., online on the screen. In addition it gives the possibility to store these values on a disk and to evaluate the saved parameter sets by displaying them in a graphical manner.

4. Test Program

A first testing of the complete controller system under realistic wind tunnel conditions was performed in Februar/March this year. The wind tunnel occupation was restricted to five days so that a very strong program was the consequence. The Tables 1 and 2 give an overview to the individual test points. The numbers reflect the amount of measured and recorded runs.

In the left columns the different test procedures are indicated while the first row contains the wind tunnel speed. Table 1 shows the runs at 'trimmed level flight conditions'. This is a more empiric assumption because it is nearly impossible to get the same conditions with a model in the wind tunnel as with a real helicopter in free flight. There are many parameters which influences the results in this case. In Ref. [5] some aspects of model rotor testing are discussed.

The adjustment we have chosen is a scaled thrust at given collective blade pitch (e.g. the same as the full scale helicopter) and roughly zero control moments (first flapping eq. zero), Fig. 11. Variations from this conditions are the test points registered in Table 2.

From the tables one can see that a major part of the runs was made to identify the T-matrix (-> T_{ident}) and the system step response (-> step). These are tests with open loop conditions. The procedure for T-matrix identification was the same as described in Ref. [6]. A stepwise phase variation of each harmonic (3/rev to 5/rev) in the range of 360 degree was used to get one dataset.

For the case of step inputs the HHC controller works in a special mode. The typical step amplitude was about 0.3 degrees. All other runs shown in the tables are closed loop conditions. As

discribed in chapter 2 we have used a 'local model minimal variance controller'. A part of these tests was made with T-matrix adaption, the rest with fixed gain. In the tables one can find these rows indicated with 'ad' respective 'fg'. One also can find these test points at steady and unsteady controller- or rotor trim conditions. In the next chapters some of the typical results will be presented.

5. Test Results

5.1 Reference Data

The dynamic characteristic of a rotor can be measured by different sensors. Each sensor gives an individual correlation with the existing vibration. To demonstrate the specific response of the model rotor three different sensor outputs are discussed. Typical sensors for vibration measurements are accelerometers. The output, e.g. scaled in g's, gives directly the vector of the corresponding vibration condition. In Fig. 12 the measured accelerations in x, y, z-direction at the hub are shown. Only the 4/rev components are plotted. One can see the typical variation with increasing speed and a minimum at roughly 60 m/s. At low speed we have the maximum vibration caused by the induced downwash distribution. It shows also the dominance of the in-plane vibrations. Because we have a distance between hub and the sensor level (roughly 20 cm) this vibrations could also be caused by vibratory moments.

The next example in Fig. 13 shows the corresponding blade flapping moments at $x = 0.15$. As expected the 2/rev part increases with the cruising speed, an effect of the periodic coefficients in the blade forcing terms. But in this Figure one can also see the dominance of the 3/rev blade flapping moments at low speed. There is a good correlation between vibration and 3/rev blade flapping versus the cruising speed. It seems that this rotor responses mainly with his first and second flapping mode which indicates, that the vibrations are not the result of only the higher modes. This validates one assumption made in Ref. [7] for analytical investigations.

The computation of the feed back gains for the minimum variance controller requires a proper quality criterion. One possible set of feed back signals are the piezo electric force transducers of the balance (chapter 3). The calculated value of the quality criterion is shown in Fig. 14. Here again a good correlation with the vibration in Fig. 12 is visible.

5.2 T-Matrix Estimation

A special objective of the tests was the T-matrix estimation. In the past many authors have made very different discourses to the T-matrix variation, e.g. depending on the cruising speed. It can be shown that the T-matrix is the transfer function of the plant between the force input (rotor blades) and the sensor location (e.g. Ref. [7]). Normally the transfer function of a rotor system varies with speed due to the changing aerodynamic damping and stiffness coefficients. A further variation appears in very extrem conditions where stall, large Mach effects, or other nonlinear behaviour occurs.

In Fig. 15 to Fig. 17 typical measured T-matrix elements are plotted. The amplitude-phase notation is used for discribing the complex values. Now it becomes visible that the gain varies in a wide range while the phase lag is nearly constant. Fig. 17 is only one example but represents the general behaviour. Similar results could be obtained from untrimmed flight conditions. One result derivable from this measurements is a controller with only an adaptive gain algorithm. This is a much more simpler task because no phase information is necessary. For example a well known RMS meter could be used.

5.3 Vibration Reduction at Steady Flight Conditions

At steady flight conditions it is possible to reduce the vibrations with manual controlled amplitude and phase of the different IHC signals Ref. [6]. This is the best condition for the adaptive closed loop system too, because the system state does not change. In Fig. 18 the results from these tests are plotted. The comparison with the basic results shows a really good performance over the range of speed. We should remember that $GF = \sqrt{J}$. This scaling results in a technical dimension e.g. the length of a vector. But it does not give such impressive differences in the results as a J scaling. The second special configuration in this Figure is the only 3/rev IHC. During the test different combinations of IHC inputs (3+5, 4+5, 3+4+5 rev) have been analysed. The quick look to the results shows clearly only a marginale improvement (additional 1 to 5 %) with additional IHC inputs.

A comparison of the blade flapping moments in Fig. 19 and 20 gives an explanation for the success of the 3/rev controller. The blade bending moments are reduced to less than 1 Nm even for the 4/rev component which yields to very low vibrations. The next Figures (21 and 22) concerne to the controller performance after enabling the system. Two different configurations are shown. In Fig. 21 the adaptive controller is enabled at level flight conditions and 20 m/s tunnel speed. This is the case with the nearly highest vibration level.

Whereas the quality criterion GF is already reduced by 30% after the first controller cycle, the T-matrix identification is obviously improved during the next steps so that the maximum reduction (80 %) can be achieved after eight cycles. A low overshot follows but the controller works stable and smooth. One must point out here the very hard conditions at 20 m/s. The algorithm was internally limited to 0.20 degrees/step which requires at least four steps to reach the required amplitude in this case.

As the adaption algorithm delivers a nearly steady T-matrix during these tests it is possible to disable the adaption and work with a constand feed back matrix (fixed gain) without any instable controller response. Even variations of the flight conditions are possible. In Fig. 22 the response of the fixed gain controller is plottet after engaging the system. It works not so smoothly as with adaption. Especially after the transition phase an oscillating controller output appears. This is a typical behaviour of a minimal variance controller because this type works at the stability boundaries (maximum feed back gain). The combination with a gain adjustment (adaption) yields to a smooth and stable working regulator.

5.4 Vibration Reduction at Variing Flight Conditions

A real helicopter must operate in various flight conditions and therefore it was a part of the wind tunnel test program to simulate some transition phases. The plot in Fig. 23 shows the controller performance during a nose up maneuver. Only a small increasing of the quality criterion becomes visible. The adaptive controller responses with small variation in the 3- and 4/rev during transition.

Deceleration is another important transition phase in the flight envelope. But for a manual controlled test rig in the wind tunnel it is nearly impossible to get a continously simulation. Therefore we made a stepwise variation of the state, with trim adjustments which consumes a few seconds after each step. The plot in Fig. 24 shows the results without these trim phases. In the whole range of speed the continously operating controller works with a good performance. The quality criterion here shown is related to the case "IHC off" to give a qualitative value of the performance.

6. Conclusions

Recent wind tunnel runs with the rotor test rig have shown that a digital adaptive feed back system is capable to reduce the vibrations in a wide range of the envelope. The Kalman filter adaption algorithm and the minimum variance controller with the local model works in conjunction with a limitation of the control step size as a smooth controller with good efficiency. Due to the specific characteristic of the four bladed hingeless model rotor and the test rig one gets some specific results as a good vibration reduction by a 3/rev IHC and small variations in the phase shift of the transfer functions (T-matrix).

An overall conclusion can be made with the following statements:

- Full digital implementation of a frequency domain controller is possible.
- Good vibration reduction can be achieved by 3/rev control.
- Different sensors which are able to observe the state can be used for feed back with the same control algorithm.
- The adaptive controller works stable in the whole envelope.
- The next generation of controller will have a gain adaption only.

7. References

[1] Reichert, G. *"Helicopter Vibration Control - A Survey"* Sixth European Rotorcraft Forum, Bristol, England 1980, Paper No. 10

[2] Mookerjee, P., Molusis, J.A., Bar-Shalom, Y. *"An Investigation of Adaptive Controllers for Helicopter Vibration and the Development of a New Dual Controller"* Nasa Contract Report 177377, University of Connecticut, 1986

[3] Lehmann, G. *"Entwurf einer rechnergestützten höherharmonischen Steuerung für den DFVLR Rotorversuchsstand"* DFVLR-IB 111-81/13, Braunschweig, 1981.

[4] Kube, R. *"Ein Rechnersystem für die höherharmonische Steuerung und Regelung eines Modellrotors"* DFVLR-IB 111-88/33, Braunschweig, 1988

[5] Langer, H.J. *"Aspects of Wind Tunnel Interference Effects on Rotor Model Loadings"* Thirteenth European Rotorcraft Forum, Arles, France, Sept. 1987, Paper No. 12.2

[6] Lehmann, G. *"The Effect of HHC to a Four Bladed Hingeless Model Rotor"* Tenth European Rotorcraft Forum, The Hague, The Netherlands, Aug. 1984, Paper No. 64

[7] Lehmann, G. *"Untersuchungen zur höherharmonischen Rotorblattsteuerung bei Hubschraubern"* DFVLR-FB 87-36, 1987

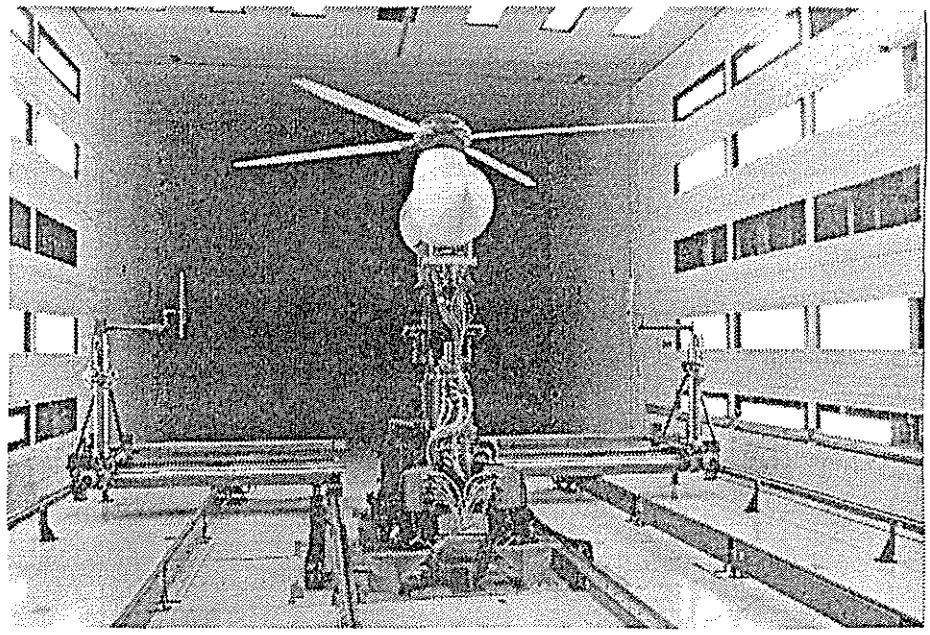

Figure 1. DFVLR-Rotor Test Stand in German-Dutch Wind Tunnel (DNW)

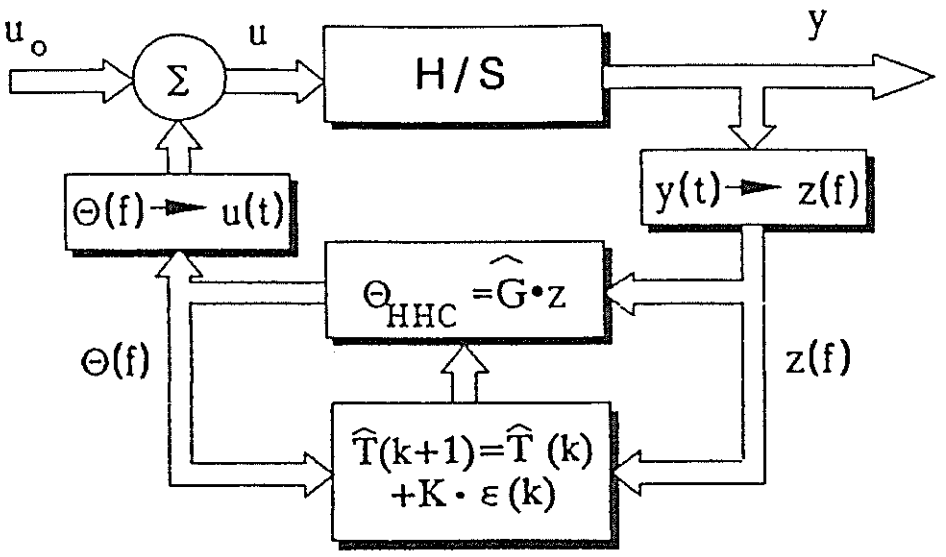

Figure 2. Schematic of the Controller

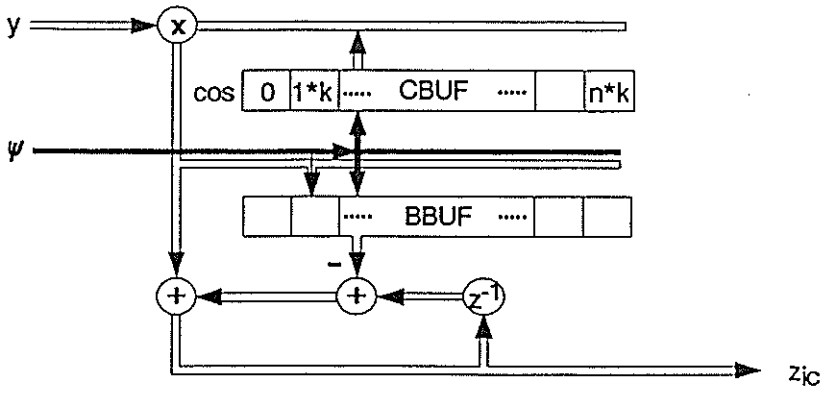

Figure 3. Time to Frequency Domain Conversion of the 4/rev Sensor Inputs

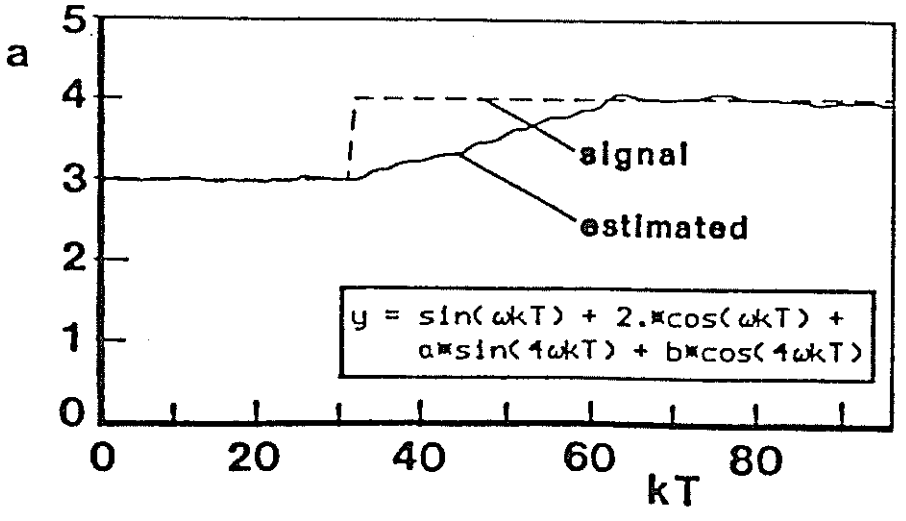

Figure 4. Simulation Result of the Conversion Algorithm

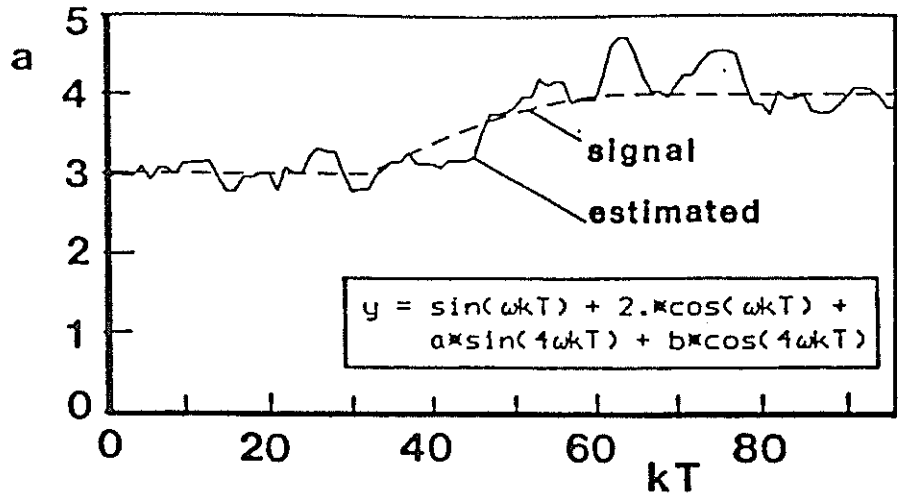

Figure 5. Simulation Result of the Modified Conversion Algorithm

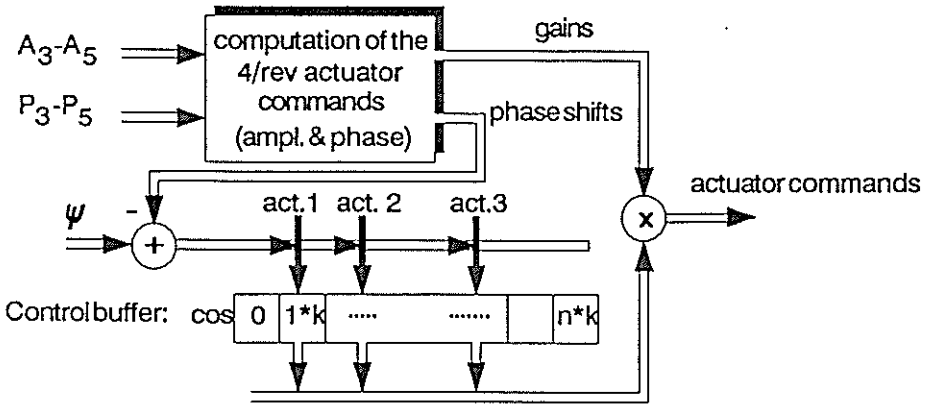

Figure 6. Frequency to Time Domain Conversion of the Regulator Output

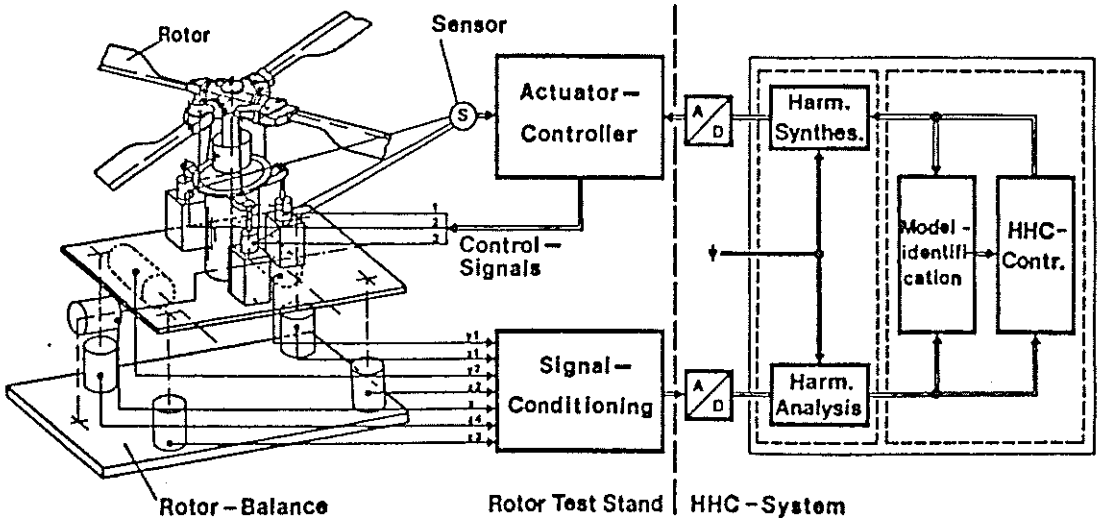

Figure 7. Schematic of the Digital HHC System

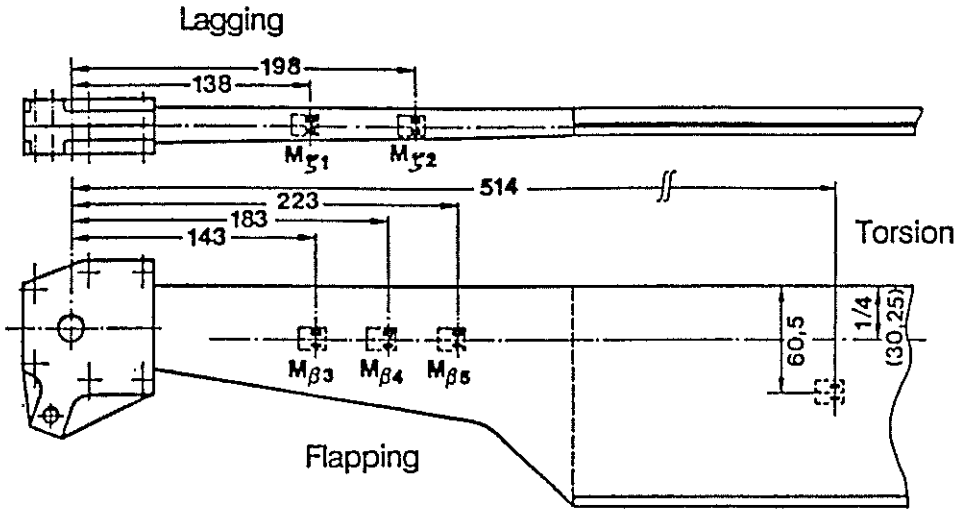

Figure 8. Sensor Locations on the Rotor Blades

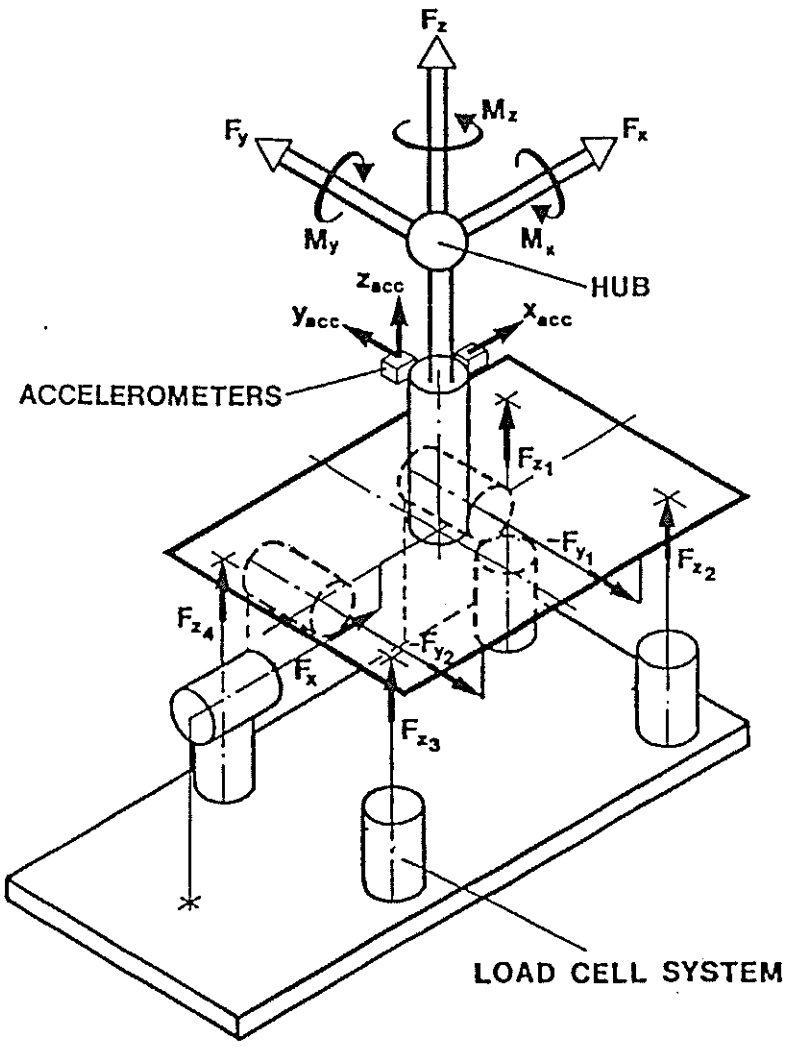

Figure 9. Sensors of the Rotor Balance

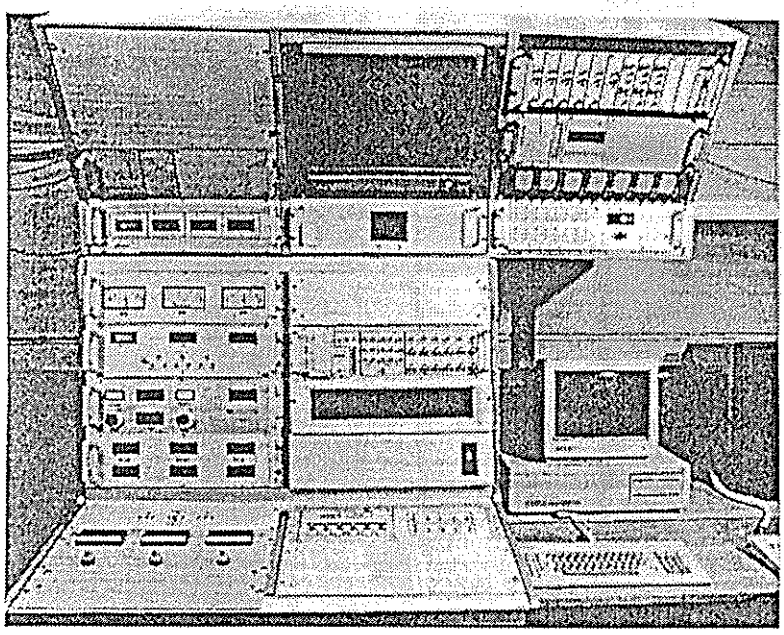

Figure 10. Computer System with Periphery

	15 m/s	20 m/s	35 m/s	50 m/s	65 m/s	70 m/s	75 m/s
T_{ident}	48	72	110	40	40		36
c-l ad.	1	11	12	3	5	1	
c-l fg.		3	15		2		
step		7	14	21			
switch on/ad.		7					
switch on/fg.			7				

Table 1: Level Flight Conditions

	15 m/s	20 m/s	35 m/s	50 m/s	65 m/s	70 m/s	75 m/s
T_{ident}	12		36				
c-l ad.		5	9		3		
c-l fg.		4	10		2		
ALFA ad.			1				
ALFA fg.			1				
switch fg.-ad.			1				

Tabelle 2: Untrimmed Flight Condition

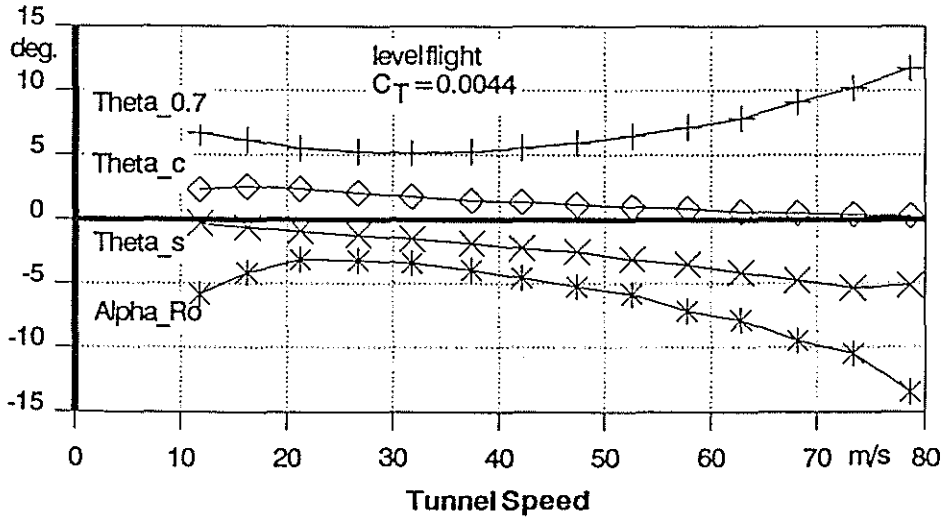

Figure 11. Trimm Conditions of the Model Rotor

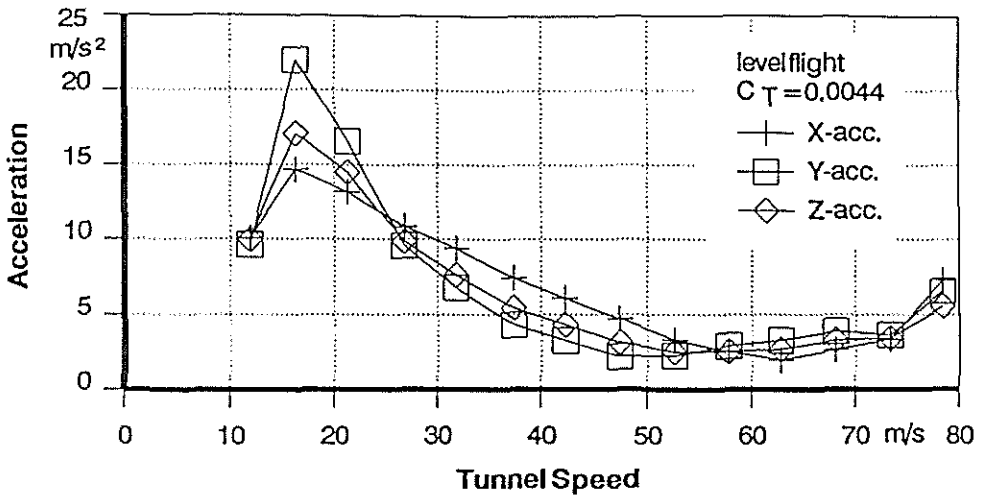

Figure 12. 4/rev Accelerations at the Rotor Shaft

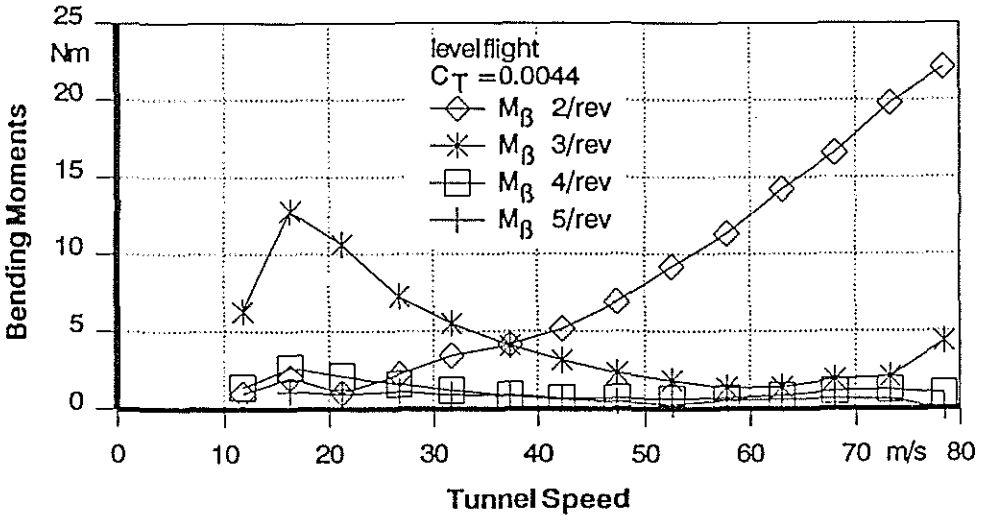

Figure 13. Blade Flapping Moments at x = 0.15

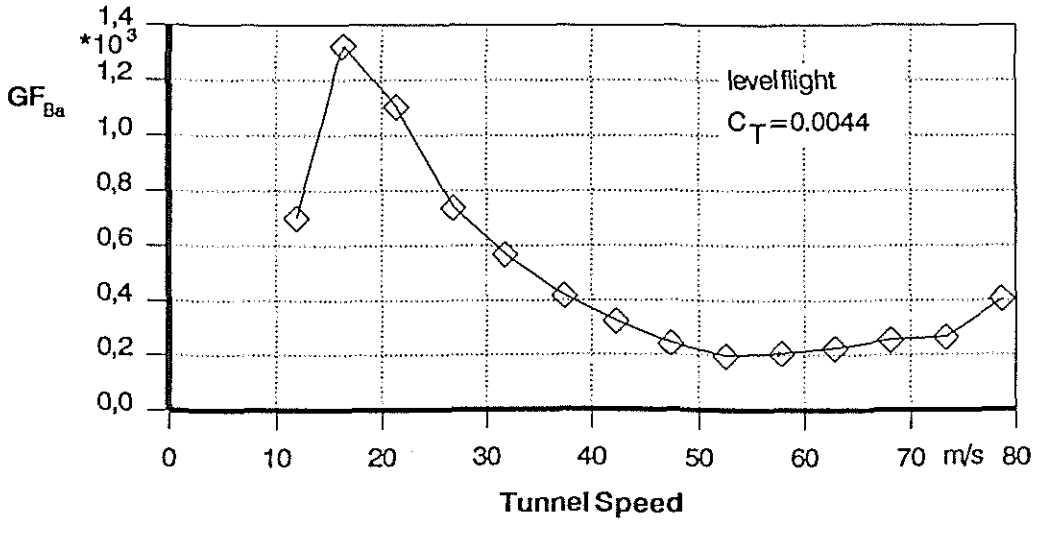

Figure 14. Quality Criterion from Balance Data

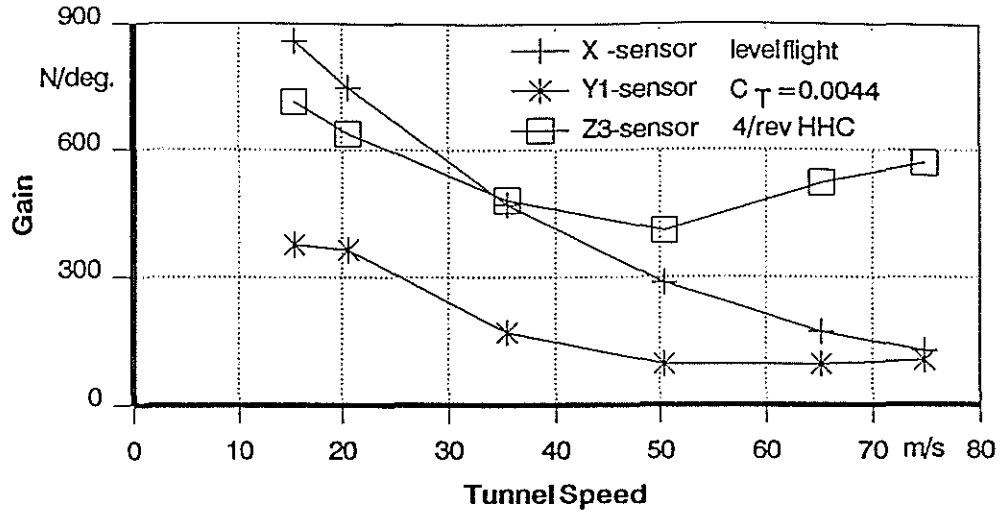

Figure 15. T-Matrix Elements of the Balance for 4/rev HHC

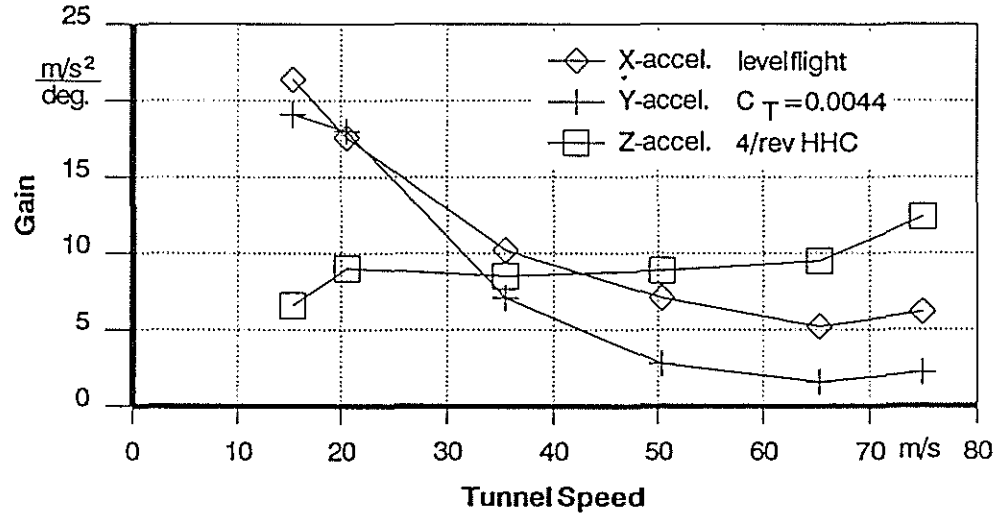

Figure 16. T-Matrix Elements of the Accelerometers for 4/rev HHC

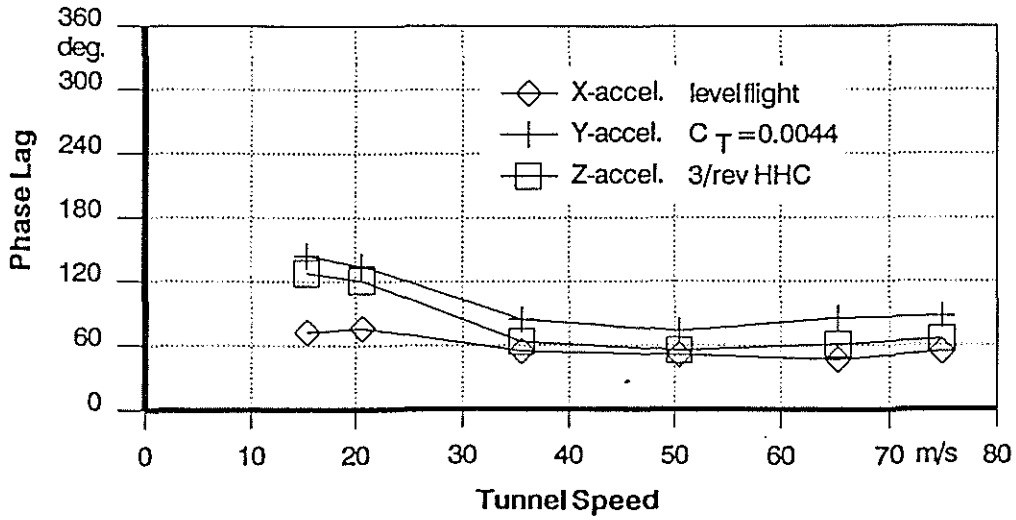

Figure 17. T-Matrix Elements of the Accelerometers for 3/rev HHC

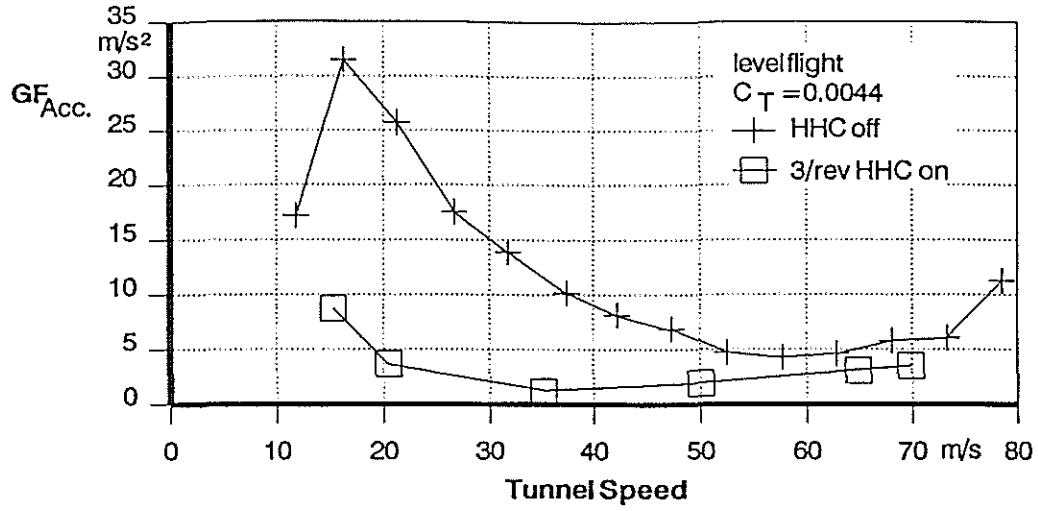

Figure 18. GF without and with HHC at Level Flight, adaptive closed loop, 3/rev

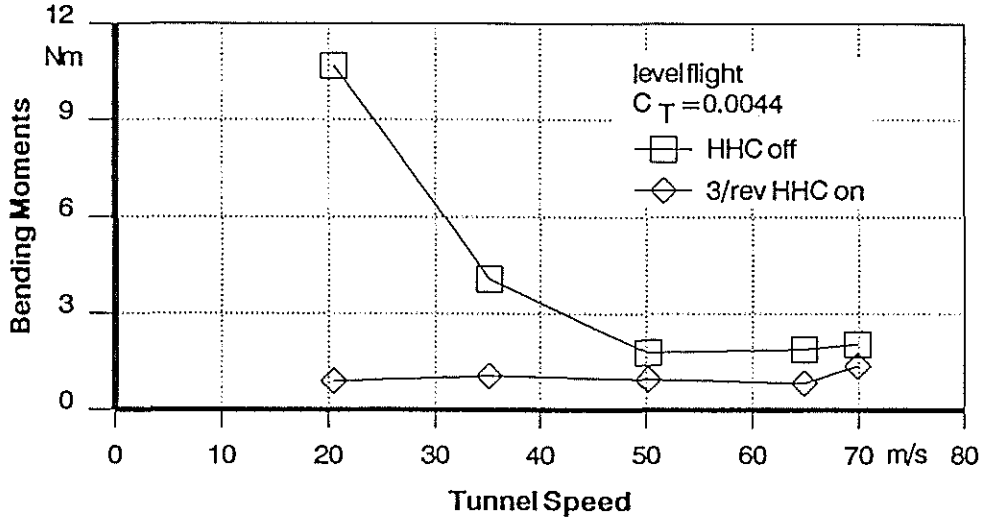

Figure 19. Blade Flapping Moments (3/rev) at x = 0.15

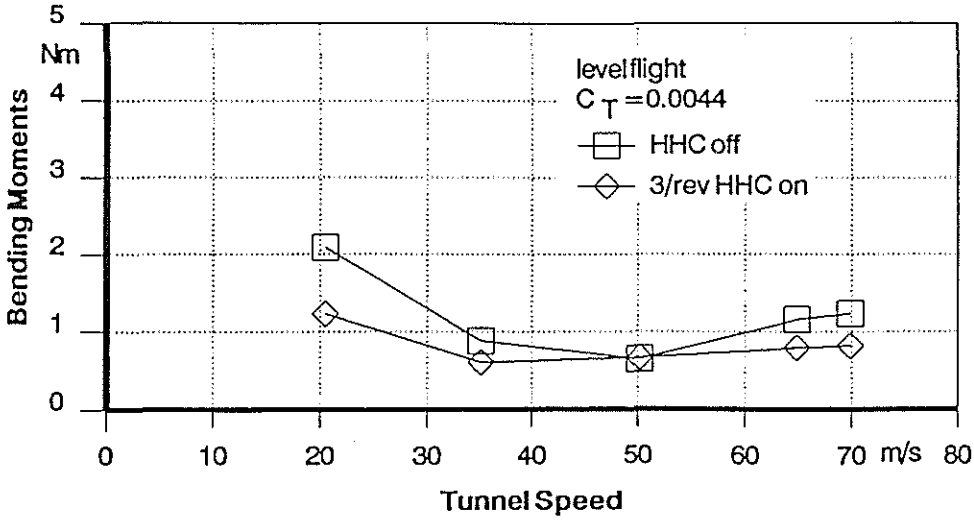

Figure 20. Blade Flapping Moments (4/rev) at x = 0.15

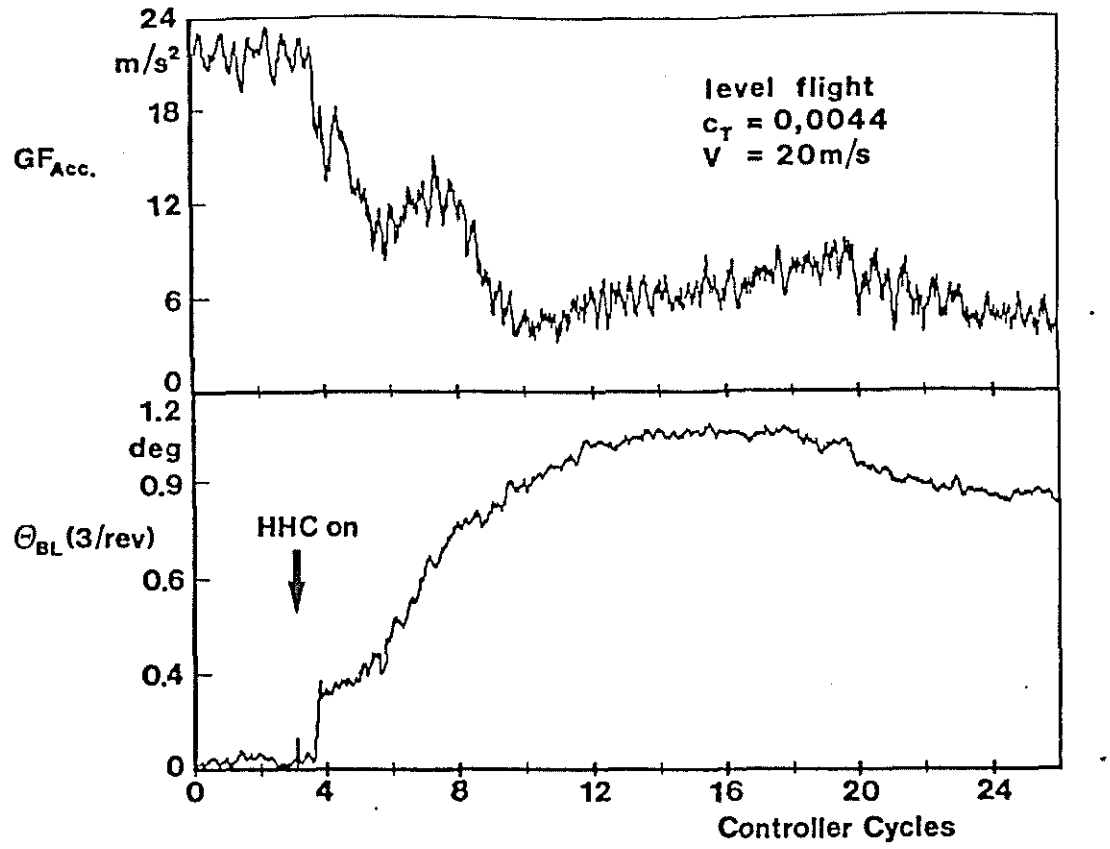

Figure 21. Performance of the Adaptive Controller after "HHC on"

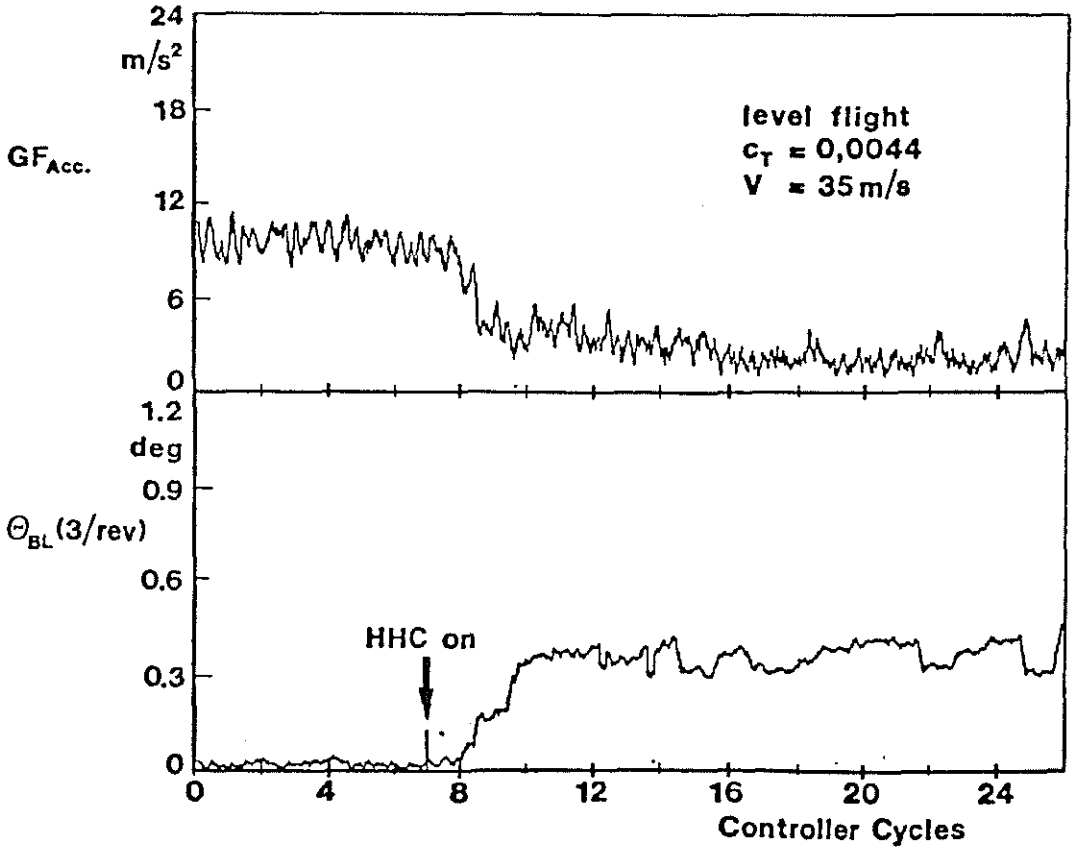

Figure 22. Performance of the Fixed Gain Controller after "HHC on"

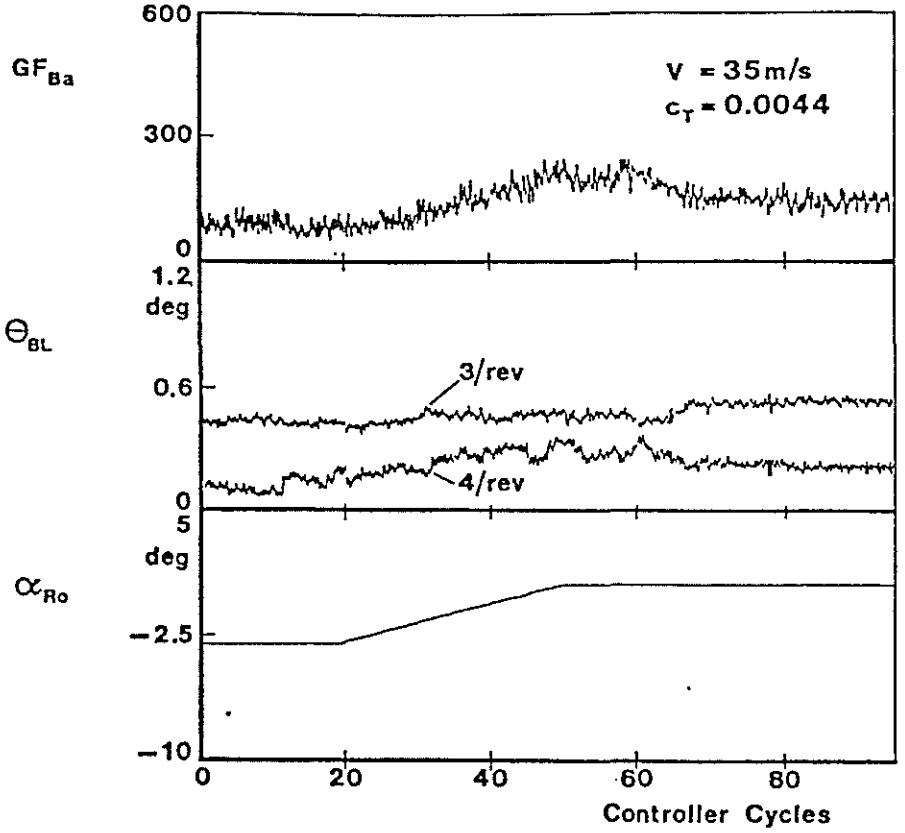

Figure 23. Performance of the Adaptive Controller during α_{Ro}-Variation

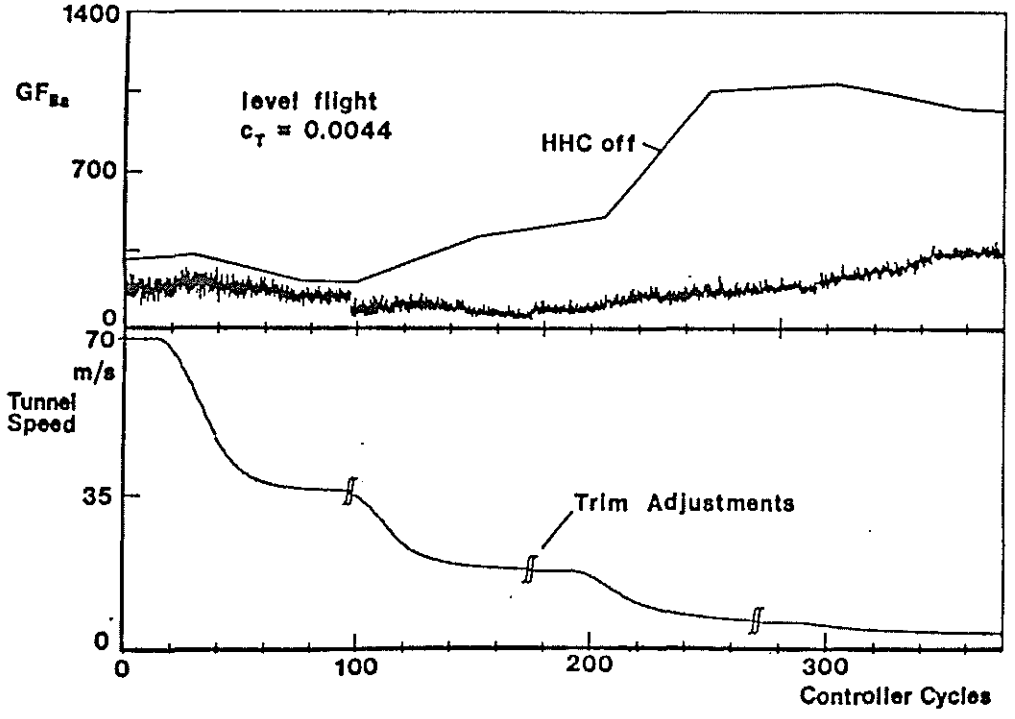

Figure 24. Performance of the Adaptive Controller during Tunnel Speed Variation